Journal of Materials Chemistry A

ROYAL SOCIETY OF CHEMISTRY

PAPER

View Article Online
View Journal | View Issue

Check for updates

Cite this: J. Mater. Chem. A, 2022, 10, 15535

Influence of amorphous carbon interlayers on nucleation and early growth of lithium metal at the current collector-solid electrolyte interface†

Moritz H. Futscher, ‡*[a] Thomas Amelal,‡[b] Jordi Sastre, [a] André Müller,[a] Jyotish Patidar,[b] Abdessalem Aribia,[a] Kerstin Thorwarth,[b] Sebastian Siol[b] and Yaroslav E. Romanyuk [a]

Received 8th April 2022
Accepted 29th June 2022

DOI: 10.1039/d2ta02843c

rsc.li/materials-a

Nucleation and early growth of Li metal is critical to the performance of anode-free solid-state batteries. We report the use of amorphous carbon deposited by direct current magnetron sputtering as an intermediate layer between the Cu current collector and the Lipon solid electrolyte. The density, conductivity, and microstructure of the carbon interlayer are varied and their influence on the reversible formation and removal of the Li metal anode is investigated. It is shown that thin films of amorphous carbon act as seed layers, reducing the overpotential for Li plating and increasing the critical current density for Li plating and stripping from 2 up to 8 mA cm^{-2}. It is further demonstrated that the ionic conductivity of the Li ions in the carbon interlayers determines their optimum thickness to be 100 nm or less, and that the initial Li loss due to interphase formation can be reduced to a few tens of nm by decreasing the density of the carbon films.

Introduction

One of the greatest improvements of solid-state batteries (SSBs) over conventional Li-ion batteries is expected to come from the use of metallic Li as an anode.[1,2] However, non-uniform plating and stripping of Li leads to current focusing and the formation of dendrites during cycling, which eventually leads to a short circuit.[3] Moreover, the use of Li-metal foils in SSBs is impractical from the manufacturing point of view and requires handling in an inert atmosphere, which may hinder eventual commercialisation.[4] An anode-free design brings the advantages of Li-metal anodes but with a significantly simplified manufacturing process due to the absence of the anode in as-manufactured cells.[5] In anode-free SSBs, the Li metal anode is reversibly formed and removed during charging and discharging. Nucleation and early growth behaviour of Li-metal is therefore of critical importance for anode-free SSBs.[6]

In 2020, Samsung revealed an anode-free SSB based on a sulfide-based electrolyte with energy density >900 Wh L^{-1}.[7] In that work, the anode-free design was enabled by an Ag–C composite layer with a thickness of about 10 μm employed between the solid separator and a current collector. Similarly, Feng *et al.* have shown that thin films of amorphous carbon deposited by thermal-decomposition vapour deposition stabilizes the interface between Li metal and garnet-based solid electrolytes.[8] They found that the amorphous structure of low graphitized carbon performed better compared to high graphitized carbon due to enhanced Li transport and a resulting lower interfacial resistance. Chen *et al.* investigated the use of hard carbon as an interlayer between solid electrolyte and anode.[9] Hard carbon consists of a highly irregular and disordered structure that provides pathways for Li transport. They found that hard carbon improves the wettability of the interface between garnet-based solid electrolytes and Li metal, and increases the critical current density and cycling performance of anode-free SSBs. While these works clearly show the promise of using carbon-based interlayers for anode-free SSBs, many questions remain about the desired properties of such an interlayer.

In this work, we investigate the use of amorphous carbon thin films deposited by direct current magnetron sputtering (DCMS) as interlayers between the Cu current collector and the lithium phosphorus oxynitride (Lipon) solid electrolyte. By varying the deposition temperature, this allows us to vary the density, microstructure, and electronic and ionic conductivity of the carbon films over a wide range. We show the influence of different material properties of the carbon interlayer on initial Li loss, overpotential, optimal interlayer thickness, and critical current density during Li plating and stripping. We find that the

[a]Laboratory for Thin Films and Photovoltaics, Empa – Swiss Federal Laboratories for Materials Science and Technology, Überlandstrasse 129, 8600 Dübendorf, Switzerland. E-mail: moritz.futscher@empa.ch

[b]Laboratory for Surface Science and Coating Technologies, Empa – Swiss Federal Laboratories for Materials Science and Technology, Überlandstrasse 129, 8600 Dübendorf, Switzerland

† Electronic supplementary information (ESI) available. See https://doi.org/10.1039/d2ta02843c

‡ Authors contributed equally to this work.

amorphous carbon interlayer reduces the overpotential for Li plating by acting as a seed layer and increases the critical current density for Li plating and stripping from 2 up to 8 mA cm^{-2}.

Results and discussion

The properties of the sputtered amorphous carbon thin films deposited at different temperatures are summarized in Fig. 1. Raman spectra of the carbon films are shown in Fig. 1a. The peaks located at about 1350 and 1590 cm^{-1} correspond to the D and G bands, respectively.[10] The D band corresponds to a breathing mode of sp^2 atoms in rings that are not connected in chains, while the G band corresponds to the stretching vibration of neighboring sp^2-bounded carbon atoms in both rings and chains. Upon heating, the ratio of the D peak intensity to G peak intensity increases, indicating an increase of the sp^2/sp^3 ratio.[10] This is further correlated with a shift in the position of the G peak to higher frequencies. The increase in sp^2/sp^3 ratio results in an increase in electronic conductivity from 5 to 29 S cm^{-1} for carbon films deposited without heating and at 350 °C, respectively (Fig. 1b). In addition, Rutherford Backscattering Spectrometry measurements show a decrease in density upon heating (Fig. 1c), which is accompanied by an increase in surface roughness and grain size (Fig. 1d–f).

To investigate the electrochemical behavior of the carbon films, we fabricate half-cells consisting of Cu/C/Lipon/Li (see Fig. 2a). We chose Lipon as the solid electrolyte because it forms a thin and stable passivation layer with Li metal and Li loss during subsequent cycling is minimal.[11,12] The amorphous nature of Lipon furthermore allows the effects of surface (electro)chemistry to be isolated from other phenomena that limit the critical current density. In crystalline solid electrolytes such as lithium lanthanum zirconium oxide (LLZO), the presence of grain boundaries increases the density of defects at the current collector-solid electrolyte interface, which by itself can lead to the formation of dendrites.[13] In addition, reversible cycling of Li has already been demonstrated in anode-free SSBs using Lipon as a solid electrolyte and Cu as a current collector.[14,28] Therefore, Lipon is an ideal candidate for the study of interlayers for anode-free SSBs, where there is little effect from the presence of the solid electrolyte. However, note that we cannot exclude any side reactions on the carbon layer during Lipon deposition. While there are reports of carbon coatings on Li metal anodes improving the performance of batteries with liquid electrolytes,[15] we were not able to measure the performance of amorphous carbon coatings deposited by DCMS with liquid electrolytes due to the deterioration of the carbon layer during plating and stripping, similar to previous results by Genovese *et al.*[16]

We cycle the cells between 0.3 and 0.0 V against Li/Li^+ at a constant current density of 0.02 mA cm^{-2}, revealing the intercalation of lithium cations into the carbon films (see Section S1 in the ESI† for details).[17] The obtained discharge capacity of the carbon films is shown in Fig. 2b. We find that the capacity decreases from about 80 mA h g^{-1} for unheated films to less than 25 mA h g^{-1} for films deposited at 350 °C. A similar capacity drop after post-annealing of sputtered amorphous carbon films has previously been observed when using liquid electrolytes.[18]

To obtain the ionic conductivity of the films, we employ impedance spectroscopy measurements. Fig. 2c shows the obtained impedance spectroscopy measurements obtained at 0.1 V against Li/Li^+. The first semicircle at high frequencies corresponds to the ionic resistance of the Lipon solid electrolyte, which has a conductivity of $3 \cdot 10^{-6}$ S cm^{-1}, the second

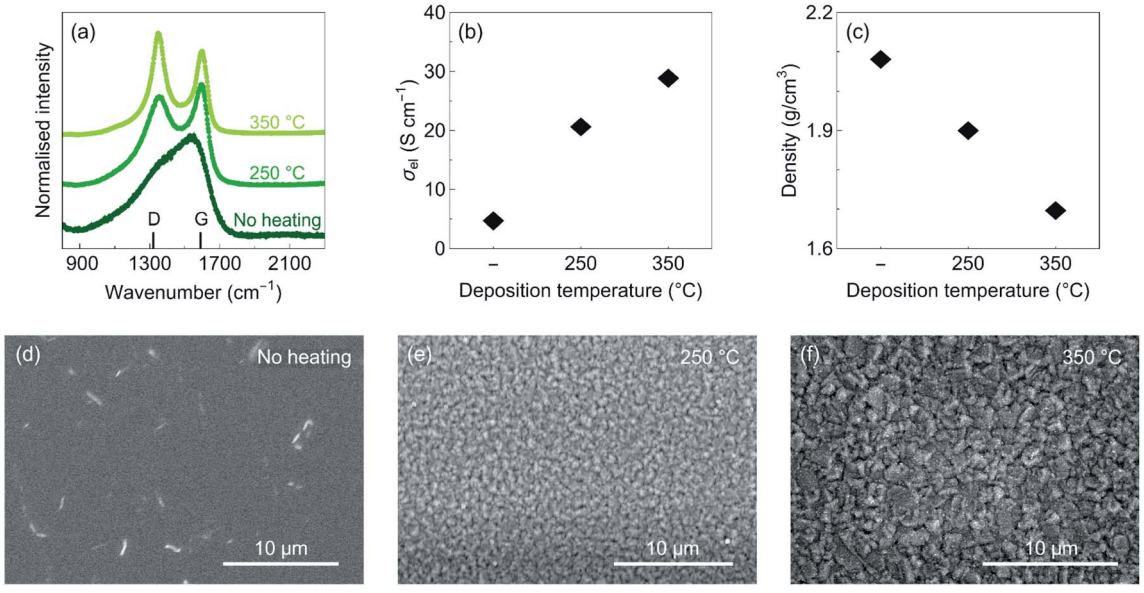

Fig. 1 Properties of sputtered amorphous carbon thin films. (a) Raman spectra, (b) electronic conductivity, (c) density, and (d–f) scanning electron microscope (SEM) micrographs of carbon films deposited without heating, at 250 °C, and at 350 °C with a thickness of 150 nm. The root mean square roughness of the films shown in (d)–(f) is 2, 29, and 36 nm, respectively.

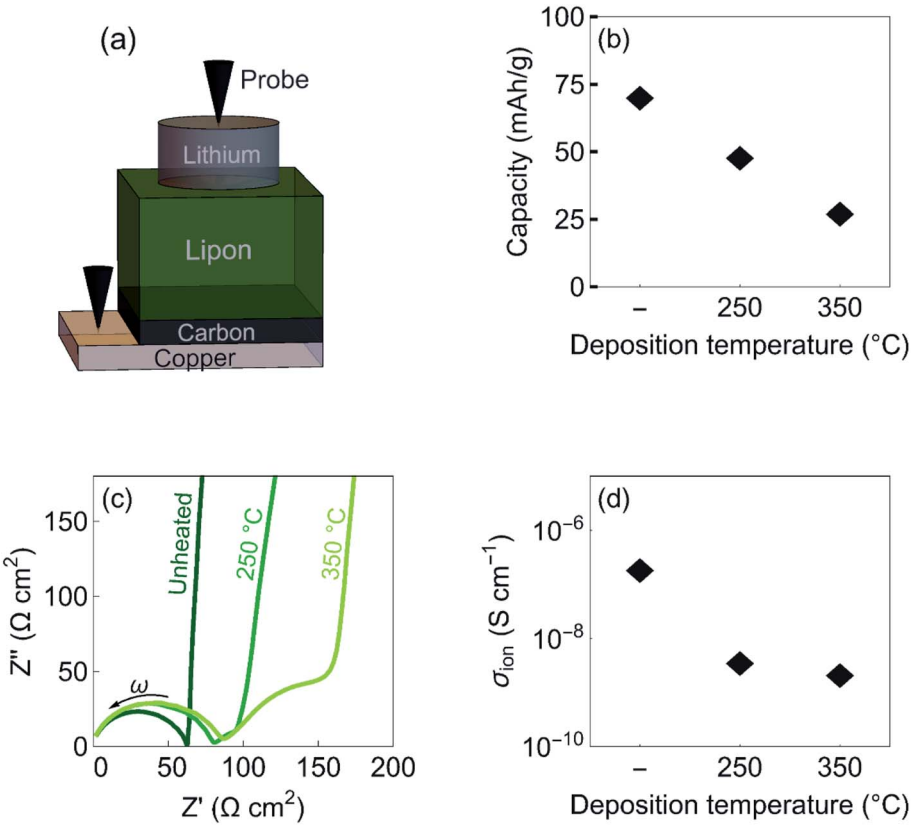

Fig. 2 Properties of lithiated amorphous carbon thin films. (a) Schematic illustration of the device configuration consisting of Cu/C/Lipon/Li. (b) Discharge capacity, (c) impedance spectroscopy measurements, and (d) obtained ionic conductivity of carbon films deposited at room temperature, at 250 °C, and at 350 °C with a thickness of 100 nm. The discharge capacity in (b) corresponds to the capacity between 0.0 and 0.3 V against Li/Li$^+$. The direction of the frequency (ω) in (c) from low to high is indicated by an arrow. The ionic conductivity is obtained with impedance spectroscopy at 0.1 V against Li/Li$^+$ (see section S2 in the ESI† for details).

semicircle corresponds to the ionic resistance of the carbon layer, and the tail at low frequencies to interface polarization. The resistance of the Lipon layer increases upon depositing Lipon on carbon layers sputtered at elevated temperatures. We attribute this increase in resistance to the increase in roughness of the substrates (see section S2 in the ESI† for details). The equivalent circuit used to fit the impedance spectra along with the fits are shown in Fig. S2 in the ESI.† We find that, in contrast to the electronic conductivity, the ionic conductivity decreases from 10^{-7} to 10^{-9} S cm^{-1} for carbon films deposited at room temperature and 350 °C, respectively (Fig. 2d). We attribute this reduction in ionic conductivity to a reduction of density of the films. In addition, the increase in grain size could also lead to a decrease in ionic conductivity.[19] Thus, we conclude that the electronic conductivity is governed by the sp^2/sp^3 ratio, while the ionic conductivity depends on the morphology of the carbon films.

To investigate the use of the carbon films as interlayers for anode-free SSBs, we plate and strip 1 μm of Li metal using a constant current density of 0.2 mA cm^{-2}. Fig. 3a shows the voltage profile for Li plating on bare Cu. After applying the current, the voltage quickly drops below 0 V against Li/Li$^+$. In contrast, the voltage profiles of the different carbon interlayers (Fig. 3b and d) show a slower decrease in voltage. This initial voltage decay corresponds to the lithiation of the carbon films. After 0 V is reached, the voltage dips before reaching a constant voltage plateau. The magnitude of the voltage plateau, often referred to as plateau overpotential, corresponds to the combined ionic resistances of the Lipon and the carbon layer. The difference between the voltage plateau and the minimum of the voltage dip corresponds to the nucleation overpotential. Here we refer to nucleation overpotential as overpotential. For bare Cu, the overpotential is around 100 mV, similar to previous reported values for Li plating on Cu.[20] After carbon deposition, the overpotential drops to about 10 mV at thicknesses greater than 50 nm (see Fig. 3e). The overpotential is similar for all carbon films deposited at different temperatures, except for the film deposited at 350 °C, which shows an increase at thickness of 150 nm (see section S3 in the ESI† for details). We note that there is a small difference between the observed overpotential for pure copper films, possibly related to the difference in surface morphology (see Fig. S3 in the ESI†).

According to the nucleation and growth theory, the observed overpotential corresponds to the potential required to overcome a nucleation barrier.[21] The region before the negative voltage peak corresponds to the formation of Li nuclei, and the following voltage plateau to the growth of Li metal. For heterogeneous nucleation, such as at the current collector-solid

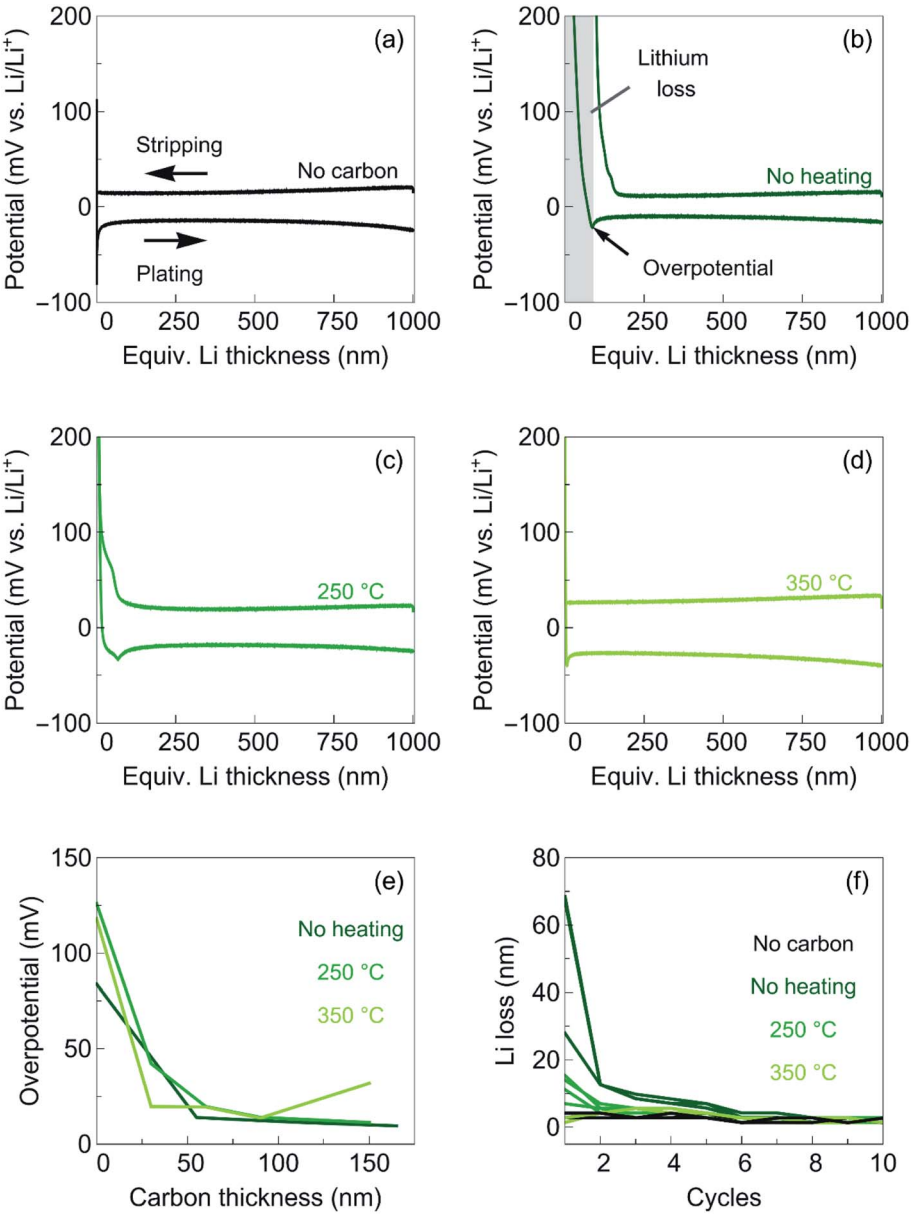

Fig. 3 Effect of carbon interlayers on plating and stripping of Li metal. Plating and stripping of 1 μm of Li between the current collector and the solid electrolyte at a current density of 0.2 mA cm^{-2} (a) without carbon, and with carbon films deposited (b) without heating, (c) at 250 °C, and at (d) 350 °C. (e) Overpotential for Li plating as a function of carbon thickness. (f) Li loss during repeated plating and stripping of Li metal. The first five cycles were performed at a current density of 0.2 mA cm^{-2} and the following at 0.4 mA cm^{-2}.

electrolyte interface, the nucleation site density is proportional to the cubic power of overpotential.[21] This behavior has been verified for the Cu/Lipon interface.[20,22] If a layer in which Li has a solubility is placed between the current collector and the solid electrolyte, it can act as a seed layer offering a vast number of initial nucleation sites.[23] Many different materials such as Au, Ag, or 3D graphitic carbon foam have been shown to act as seed layers and reduce the overpotential, facilitating homogeneous Li plating and stripping the likelihood of Li dendrite formation.[23–25] Hence, our results show that amorphous carbon layers can act as initial seed layer for a uniform Li plating with a low initial overpotential.

In addition to the magnitude of the voltage dip, a change in the position of the voltage dip is observed. For the carbon films deposited without heating and at 350 °C, the voltage dips occur shortly after 0 V is reached. In contrast, for the carbon film deposited at 250 °C, the voltage stays at a negative voltage for a while before a voltage dip is observed (see Fig. S4 in the ESI†). Using dynamic electrochemical impedance spectroscopy during Li deposition, Westover *et al.* found that the negative voltage region before the voltage dip corresponds to the interphase formation at the Ni/Lipon interface.[26] They observed that this interphase formation even extends slightly beyond the voltage dip. We therefore assume that the carbon films deposited at

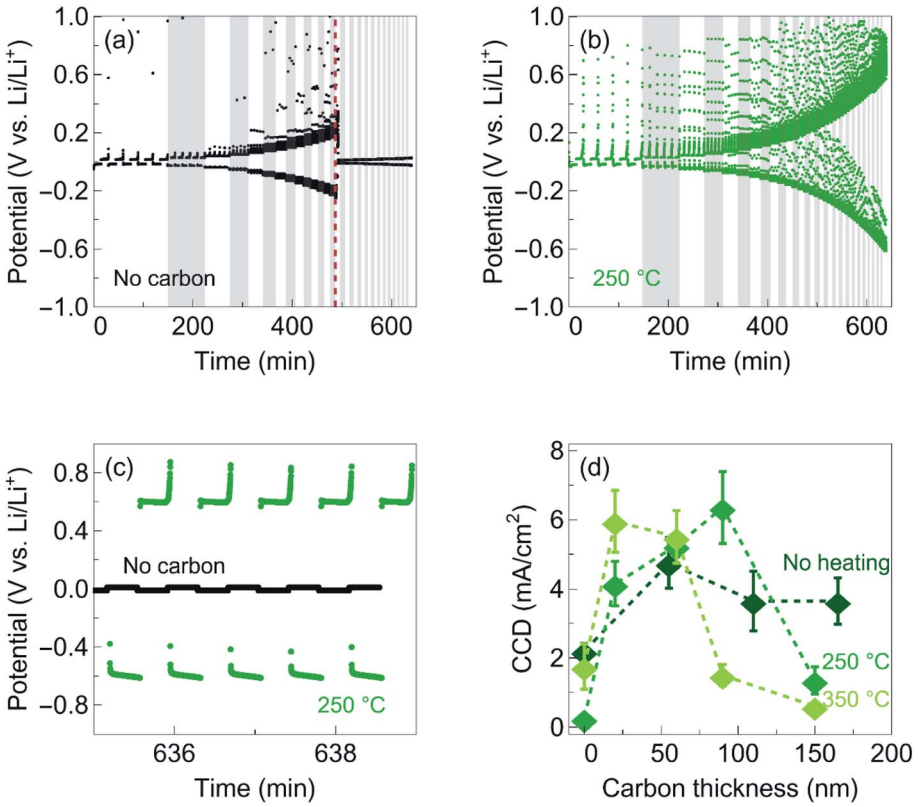

Fig. 4 Effect of carbon interlayers on the critical current density. Stripping and plating of Li metal at the current collector-solid electrolyte interface (a) without carbon and (b) with a 100 nm amorphous carbon layer deposited at 250 °C. The current density is increased from 0.2 to 8 mA cm^{-2} in steps of 0.2 mA cm^{-2}, with each current density repeated five times. The areas with different current densities are marked by shades of gray. The red dashed line in (a) shows the location where the short occurs. (c) Magnification of (a) and (b) in the time window between 635 and 639 minutes of stripping and plating at a current density of 8 mA cm^{-2}. (d) Critical current density as a function of thickness of the carbon interlayers deposited without heating, at 250 °C, and at 350 °C. Each measurement is repeated four times.

250 °C are involved in the interphase formation, which is also indicated by the reversible capacity obtained. Some interphase formation is also observed in the carbon films deposited without heating, although to a lesser extent than in the films deposited at 250 °C, which may be related to the higher lithiation capacity of the films. For the carbon films deposited at 350 °C, on the other hand, we do not observe any interphase formation. Due to the low ionic conductivity in the carbon films deposited at 350 °C and the visible crack formation (see Fig. 1f), we assume that Li deposits directly on copper. This assumption is supported by the presence of two voltage dips in these films (see Fig. S5 in the ESI†).

Upon stripping the previously deposited Li metal with the same current density of 0.2 mA cm^{-2} until a voltage of 0.8 V is reached, we found that not all of the capacitance can be reversibly recovered. Fig. 3f shows the observed Li loss during repeated cycling. The irreversible capacity loss strongly depends on the deposition temperature of the carbon films. The highest lithium loss is observed for the carbon films deposited without heating, while no lithium loss is observed for the films deposited at 350 °C. We attribute this reduction in lithium loss to the reduction in discharge capacity of the films when deposited at elevated temperatures. In addition, the functional groups on

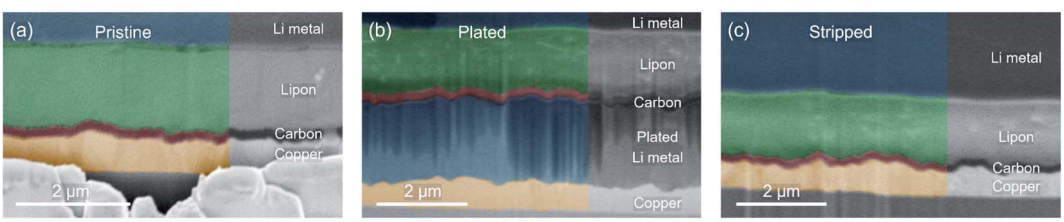

Fig. 5 Cross-sectional SEM micrographs of a carbon interlayer at the current collector-solid electrolyte interface. (a) After fabrication, (b) after plating an equivalent Li thickness of 1 μm, and (c) after subsequent stripping the plated Li. The thickness of the amorphous carbon layer is 100 nm deposited at 250 °C. Plating and stripping of Li was performed at a current density of 0.2 mA cm^{-2}.

the surfaces might change upon heating, which also can affect the irreversible capacity loss. Upon repeated plating and stripping, the initial irreversible capacitance decreases until all carbon films no longer exhibit a significant Li loss (Fig. 3f). We note that, although the irreversible lithium loss of the carbon film deposited without heating is the largest, it is still very small compared to the typical lithium losses of the best liquid organic electrolytes (a few hundreds of nm).[27]

To investigate the effect of the carbon interlayers on the critical current density for Li plating and stripping, we cycled the cells at current densities ranging from 0.2 to 8 mA cm^{-2} in steps of 0.2 mA cm^{-2} (Fig. 4a and b). Each current density was repeated for 5 times, and applied for a time corresponding to a thickness of 250 nm of Li metal to be plated/stripped. Fig. 4a shows the voltage profile as a function of time for the reference sample without carbon. As the current density is increased, the voltage increases until a short occurs. The critical current density is defined as the highest current density at which the cell can be cycled before a short circuit occurs. Upon adding a 100 nm thick carbon interlayer deposited at 250 °C, we observe a great increase in critical current density, with some cells being able to operate reversibly at current densities as high as 8 mA cm^{-2} without shorting (Fig. 4b). Fig. 4c shows the voltage profiles for plating and stripping at 8 mA cm^{-2}. Reversible plating and stripping of Li metal is observed for the cells with a carbon interlayer, while the cell without carbon is already short-circuited.

While the cells employing a 100 nm thick carbon interlayers deposited at 250 °C have the highest critical current density of 6.4 ± 1.0 mA cm^{-2} averaged over four measurements, we find that all carbon films can improve the critical current density when deposited as thin films on the order of tens of nm (Fig. 4c). At 50 nm, all the carbon layers show a similar critical current density of 5 mA cm^{-2}, more than twice the critical current density of the cells without carbon. As the thickness of the carbon layers is increased, the critical current density drops. This effect is most significant in the films deposited at 350 °C and least notable in the films deposited without heating. We attribute this difference in thickness dependence to a difference in ionic conductivity. Hence, our results show that the thicker the interlayer is, the higher the ionic conductivity needs to be. These results may explain why Ag is needed in Samsung's work to improve the ionic conductivity of Li-ions by forming Li–Ag alloys, where the carbon interlayer is on the order of a few micrometers.[7] However, a more detailed study is needed to fully understand the benefits of Ag in the Ag–C composite layer.

Fig. 5 shows cross-sectional SEM micrographs of an amorphous carbon interlayer between the current collector and the solid electrolyte after fabrication, after plating an equivalent Li thickness of 1 μm, and after subsequent stripping of the plated Li metal. We find that after plating, a dense and uniform Li metal layer is formed between the current collector and the carbon interlayer. In fact, the deposition of Li is so uniform that even after a thick layer is deposited, the structure of the current collector is maintained at the Li metal–carbon interface. In contrast, for samples without carbon, we observe a non-homogeneous plating of Li metal, which can lead to current focusing (see section S4 in the ESI†). After the subsequent stripping process, all the previously deposited Li metal is removed and the carbon layer remains between the current collector and the solid electrolyte. We note that, although the electronic conductivity of the carbon layer is much higher than its ionic conductivity, Li metal is plated below the carbon interlayer. This is in accordance with previous findings by Lee *et al.*[7] Hence, we assume that Li ions get partially reduced upon adsorption on the carbon films, and then migrate through the carbon layer before plating on the current collector surface. The migration of Li through the carbon layer further explains why the ionic conductivity of Li ions in the carbon layer is a crucial parameter affecting its optimum thickness for reversible Li plating and stripping.

To test whether the beneficial properties of the amorphous carbon interlayer can be transferred to anode-free batteries, we fabricate anode-free thin-film solid-state batteries consisting of Cu/C/Lipon/LCO/Au (see section S5 in the ESI† for details). We find that thin amorphous carbon layers deposited at 250 °C improve the discharge capacity and reduce the capacity fading compared to the reference without carbon. However, further studies on the integration of amorphous carbon films in batteries are needed to fully understand the impact on anode-free solid-state batteries.

In addition to improving the plating performance, the presence of an electronically conductive layer between the Li metal anode and the solid electrolyte might also help to improve the stripping performance by screening inhomogeneous electric fields generated by non-uniform Li stripping. We believe this is an interesting concept that merits further investigation.

Conclusions

In conclusion, we demonstrate that thin films of amorphous carbon promote homogeneous Li plating without dendrite formation at the current collector-solid electrolyte interface by acting as an initial nuclei seed layer. We show that carbon films prepared by direct current magnetron sputtering with a wide range of morphology and electronic properties all significantly improve the critical current density of Li plating and stripping when deposited as thin films on the order of tens of nanometers. The ionic conductivity of the carbon films determines their optimum thickness of 100 nm or less. Although the carbon films exhibit irreversible Li loss due to interphase formation, this loss depends on the density of the carbon films and can be reduced to a few nanometers when deposited at elevated temperatures. Our work sheds light on the properties that carbon-based interlayers must have to enable anode-free SSBs. Sputtered amorphous carbon films are of particular interest as they are only tens of nanometers thick and therefore have negligible impact on energy and power densities, while improving the nucleation and early growth kinetics of Li metal. In addition, they can be universally used between different metal anodes and solid electrolyte in anode-free SSBs, improving the applicability of SSBs.

Experimental methods

Fabrication

The amorphous carbon thin films were deposited in an AJA ATC 1500 F sputtering system (AJA International, Inc.) on borosilicate glass substrates. DC sputtering from a 2″ carbon target (graphite with a purity of 99.9%, Mo-bonded, Plansee SE) in an unbalanced magnetron was performed in Ar atmosphere at a power of 100 W, a working pressure of $4 \cdot 10^{-3}$ mbar, and a working distance of approximately 13 cm. The composition of the carbon thin films is shown in Fig. S9 in the ESI.† Prior to the deposition of the carbon films, the substrates were cleaned in an RF-generated Ar plasma at 100 V and $1.2 \cdot 10^{-2}$ mbar for 5 minutes, followed by the reactive deposition of 50 nm TiN from a Ti target (HMW Hauner, 99.995%) at 200 W in mixed Ar/N atmosphere and the deposition of 500 nm Cu (HMW Hauner, 99.99%) at 100 W without breaking the vacuum. The whole deposition procedure (RF cleaning + films) was performed without additional heating of the substrate holder, at 250 °C, and at 350 °C, respectively. Lipon with a thickness of 1 μm was deposited on the carbon films at room temperature by RF magnetron sputtering using co-sputtering of 2″ targets of Li_3PO_4 (Kurt J Lesker Co.) and Li_2O (Toshima Manufacturing Co.) in an Orion sputtering system (AJA International Inc.) in N_2 atmosphere at a power of 100 W and 150 W, respectively, and a working pressure of $4 \cdot 10^{-3}$ mbar at a working distance of approximately 13 cm. Li with a thickness of 5 μm was deposited by thermal evaporation at a rate of 25 Å s^{-1} through shadow masks with a diameter of 0.1 cm using a Nexdep evaporator (Angstrom Engineering Inc). Finally, 100 nm of Cu was deposited by thermal evaporation through the same shadow mask.

Characterization

Raman spectroscopy was performed with an alpha300 R Raman imaging microscope (WiTec) with an excitation wavelength of 532 nm and a laser power of 5 mW at 100× magnification. We have performed degradation tests with laser powers ranging from 0.5 to 30 mW, keeping the dose constant by varying the integration time. The Raman spectra remained unaffected up to a laser power of 8 mW. Shown spectra are the average of 10 accumulations of 5 seconds integration time each. The electronic conductivity was determined with a home-built four-point probe system on carbon films deposited on borosilicate glass. The thickness of the carbon thin films was determined with a stylus profilometer (Bruker DektakXT). Rutherford Backscattering Spectrometry with 2 MeV He ions and Elastic Recoil Detection Analysis with 13 MeV 127I ions were performed at the Laboratory of Ion Beam Physics at ETH Zurich to determine the area density and composition of the carbon films on Si substrates. The microstructure of the films was determined using a scanning electron microscope (Hitachi S-4800) at an acceleration voltage of 10 kV. Cross-section SEM images were obtained with a FIB/SEM Helios 600i TFS system in a cryogenic stage at an acceleration voltage of 3 kV. The topography and roughness of the films was measured using dimension icon atomic force microscope (Bruker). The image acquisition was performed in ScanAsyst mode with a silicon ScanAsyst-Air tip. Electrochemical characterization was performed in an Ar-filled glovebox at room temperature using a Squidstat potentiostat (Admiral Instruments). Impedance spectroscopy measurements were performed between 0.1 Hz and 10 MHz with an a.c. amplitude of 50 mV.

Conflicts of interest

There are no conflicts to declare.

Acknowledgements

The work is supported by the Empa internal project "a-CARBON-battery" and the Strategic Focus Area (SFA) Advanced Manufacturing of the ETH Domain (project "SOL4BAT"). M. H. F. is supported by a Rubicon Fellowship from the Netherlands Organisation for Scientific Research (NWO). J. P. acknowledges funding by the SNSF (project no. 200021_196980). M. H. F. and A. M. acknowledges funding by the SNSF (project no. 200021_172764). Support from the Laboratory of Ion Beam Physics and the Scientific Center for Optical and Electron Microscopy (ScopeM) of the Swiss Federal Institute of Technology (ETHZ) for the RBS analysis and cryo-FIB-SEM measurements, respectively, is gratefully acknowledged.

References

1 J. Liu, Z. Bao, Y. Cui, E. J. Dufek, J. B. Goodenough, P. Khalifah, Q. Li, B. Y. Liaw, P. Liu, A. Manthiram, Y. S. Meng, V. R. Subramanian, M. F. Toney, V. V. Viswanathan, M. S. Whittingham, J. Xiao, W. Xu, J. Yang, X.-Q. Yang and J.-G. Zhang, Pathways for Practical High-Energy Long-Cycling Lithium Metal Batteries, *Nat. Energy*, 2019, **4**(3), 180–186, DOI: **10.1038/s41560-019-0338-x**.

2 J. Janek and W. G. Zeier, A Solid Future for Battery Development, *Nat. Energy*, 2016, **1**(9), 16141, DOI: **10.1038/nenergy.2016.141**.

3 L. Porz, T. Swamy, B. W. Sheldon, D. Rettenwander, T. Frömling, H. L. Thaman, S. Berendts, R. Uecker, W. C. Carter and Y. Chiang, Mechanism of Lithium Metal Penetration through Inorganic Solid Electrolytes, *Adv. Energy Mater.*, 2017, **7**(20), 1701003, DOI: **10.1002/aenm.201701003**.

4 R. Schmuch, R. Wagner, G. Hörpel, T. Placke and M. Winter, Performance and Cost of Materials for Lithium-Based Rechargeable Automotive Batteries, *Nat. Energy*, 2018, **3**(4), 267–278, DOI: **10.1038/s41560-018-0107-2**.

5 R. V. Salvatierra, W. Chen and J. M. Tour, What Can Be Expected from "Anode-free" Lithium Metal Batteries?, *Adv. Energy Sustain. Res.*, 2021, **2**(5), 2000110, DOI: **10.1002/aesr.202000110**.

6 C. Heubner, S. Maletti, H. Auer, J. Hüttl, K. Voigt, O. Lohrberg, K. Nikolowski, M. Partsch and A. Michaelis, From Lithium-metal toward Anode-free Solid-state Batteries: Current Developments, Issues, and Challenges,

Adv. Funct. Mater., 2021, **31**(51), 2106608, DOI: 10.1002/adfm.202106608.

7 Y.-G. Lee, S. Fujiki, C. Jung, N. Suzuki, N. Yashiro, R. Omoda, D.-S. Ko, T. Shiratsuchi, T. Sugimoto, S. Ryu, J. H. Ku, T. Watanabe, Y. Park, Y. Aihara, D. Im and I. T. Han, High-Energy Long-Cycling All-Solid-State Lithium Metal Batteries Enabled by Silver–Carbon Composite Anodes, *Nat. Energy*, 2020, **5**(4), 299–308, DOI: 10.1038/s41560-020-0575-z.

8 W. Feng, X. Dong, X. Zhang, Z. Lai, P. Li, C. Wang, Y. Wang and Y. Xia, Li/Garnet Interface Stabilization by Thermal-decomposition Vapor Deposition of an Amorphous Carbon Layer, *Angew. Chem., Int. Ed.*, 2020, **59**(13), 5346–5349, DOI: 10.1002/anie.201915900.

9 L. Chen, J. Zhang, R. Tong, J. Zhang, H. Wang, G. Shao and C. Wang, Excellent Li/Garnet Interface Wettability Achieved by Porous Hard Carbon Layer for Solid State Li Metal Battery, *Small*, 2021, 2106142, DOI: 10.1002/smll.202106142.

10 A. C. Ferrari and J. Robertson, Raman Spectroscopy of Amorphous, Nanostructured, Diamond–like Carbon, and Nanodiamond, *Philos. Trans. R. Soc., A*, 2004, **362**(1824), 2477–2512, DOI: 10.1098/rsta.2004.1452.

11 J. B. Bates, N. J. Dudney, D. C. Lubben, G. R. Gruzalski, B. S. Kwak, X. Yu and R. A. Zuhr, Thin-Film Rechargeable Lithium Batteries, *J. Power Sources*, 1995, **54**(1), 58–62, DOI: 10.1016/0378-7753(94)02040-A.

12 J. Li, C. Ma, M. Chi, C. Liang and N. J. Dudney, Solid Electrolyte: The Key for High-Voltage Lithium Batteries, *Adv. Energy Mater.*, 2015, **5**(4), 1401408, DOI: 10.1002/aenm.201401408.

13 J. Sastre, M. H. Futscher, L. Pompizi, A. Aribia, A. Priebe, J. Overbeck, M. Stiefel, A. N. Tiwari and Y. E. Romanyuk, Blocking Lithium Dendrite Growth in Solid-State Batteries with an Ultrathin Amorphous Li-La-Zr-O Solid Electrolyte, *Commun. Mater.*, 2021, **2**(1), 76, DOI: 10.1038/s43246-021-00177-4.

14 B. J. Neudecker, N. J. Dudney and J. B. Bates, "Lithium-Free" Thin-Film Battery with *in Situ* Plated Li Anode, *J. Electrochem. Soc.*, 2000, **147**(2), 517, DOI: 10.1149/1.1393226.

15 T. Yamamoto, H. Iwasaki, Y. Suzuki, M. Sakakura, Y. Fujii, M. Motoyama and Y. Iriyama, A Li-Free Inverted-Stack All-Solid-State Thin Film Battery Using Crystalline Cathode Material, *Electrochem. Commun.*, 2019, **105**, 106494, DOI: 10.1016/j.elecom.2019.106494.

16 M. Genovese, A. J. Louli, R. Weber, R. J. Sanderson, M. B. Johnson and J. R. Dahn, Combinatorial Methods for Improving Lithium Metal Cycling Efficiency, *J. Electrochem. Soc.*, 2018, **165**(13), A3000–A3013, DOI: 10.1149/2.0401813jes.

17 J. Asenbauer, T. Eisenmann, M. Kuenzel, A. Kazzazi, Z. Chen and D. Bresser, The Success Story of Graphite as a Lithium-Ion Anode Material – Fundamentals, Remaining Challenges, and Recent Developments Including Silicon (Oxide) Composites, *Sustain. Energy Fuels*, 2020, **4**(11), 5387–5416, DOI: 10.1039/D0SE00175A.

18 R. Fathi, R. J. Sanderson, L. J. Lucas and J. R. Dahn, The Electrochemical Reaction of Lithium with High-Capacity Dense Sputtered Carbon, *Carbon*, 2014, **74**, 249–254, DOI: 10.1016/j.carbon.2014.03.029.

19 K. Zaghib, F. Brochu, A. Guerfi and K. Kinoshita, Effect of Particle Size on Lithium Intercalation Rates in Natural Graphite, *J. Power Sources*, 2001, **103**(1), 140–146, DOI: 10.1016/S0378-7753(01)00853-9.

20 M. Motoyama, M. Hirota, T. Yamamoto and Y. Iriyama, Temperature Effects on Li Nucleation at Cu/LiPON Interfaces, *ACS Appl. Mater. Interfaces*, 2020, **12**(34), 38045–38053, DOI: 10.1021/acsami.0c02354.

21 A. Pei, G. Zheng, F. Shi, Y. Li and Y. Cui, Nanoscale Nucleation and Growth of Electrodeposited Lithium Metal, *Nano Lett.*, 2017, **17**(2), 1132–1139, DOI: 10.1021/acs.nanolett.6b04755.

22 M. Motoyama, M. Ejiri and Y. Iriyama, Modeling the Nucleation and Growth of Li at Metal Current Collector/LiPON Interfaces, *J. Electrochem. Soc.*, 2015, **162**(13), A7067–A7071, DOI: 10.1149/2.0051513jes.

23 K. Yan, Z. Lu, H.-W. Lee, F. Xiong, P.-C. Hsu, Y. Li, J. Zhao, S. Chu and Y. Cui, Selective Deposition and Stable Encapsulation of Lithium through Heterogeneous Seeded Growth, *Nat. Energy*, 2016, **1**(3), 16010, DOI: 10.1038/nenergy.2016.10.

24 C. Yang, Y. Yao, S. He, H. Xie, E. Hitz and L. Hu, Ultrafine Silver Nanoparticles for Seeded Lithium Deposition toward Stable Lithium Metal Anode, *Adv. Mater.*, 2017, **29**(38), 1702714, DOI: 10.1002/adma.201702714.

25 L. Liu, Y.-X. Yin, J.-Y. Li, S.-H. Wang, Y.-G. Guo and L.-J. Wan, Uniform Lithium Nucleation/Growth Induced by Lightweight Nitrogen-Doped Graphitic Carbon Foams for High-Performance Lithium Metal Anodes, *Adv. Mater.*, 2018, **30**(10), 1706216, DOI: 10.1002/adma.201706216.

26 A. S. Westover, R. L. Sacci and N. Dudney, Electroanalytical Measurement of Interphase Formation at a Li Metal–Solid Electrolyte Interface, *ACS Energy Lett.*, 2020, **5**(12), 3860–3867, DOI: 10.1021/acsenergylett.0c01840.

27 C. Fang, J. Li, M. Zhang, Y. Zhang, F. Yang, J. Z. Lee, M.-H. Lee, J. Alvarado, M. A. Schroeder, Y. Yang, B. Lu, N. Williams, M. Ceja, L. Yang, M. Cai, J. Gu, K. Xu, X. Wang and Y. S. Meng, Quantifying Inactive Lithium in Lithium Metal Batteries, *Nature*, 2019, **572**(7770), 511–515, DOI: 10.1038/s41586-019-1481-z.

28 G. Zheng, S. W. Lee, Z. Liang, H.-W. Lee, K. Yan, H. Yao, H. Wang, W. Li, S. Chu and Y. Cui, Interconnected Hollow Carbon Nanospheres for Stable Lithium Metal Anodes, *Nat. Nanotechnol.*, 2014, **9**, 618–623, DOI: 10.1038/nnano.2014.152.

